Geopersia 2022, 12(1): 107-126
DOI: 10.22059/GEOPE.2021.327866.648628

RESEARCH PAPER

Mechanism and mode of albitization of detrital feldspar in the Devonian Padeha Formation, Eastern Alborz, Iran

Mehdi Reza Poursoltani *

Department of Geology, Mashhad Branch, Islamic Azad University, Mashhad, Iran

Received: 28 July 2021, Revised: 30 September 2021, Accepted: 12 October 2021

Abstract
The Early to Middle Devonian Padeha Formation in the Eastern Alborz includes a thick terrestrial syn-rift succession of white to purple sandstone, conglomerate and shale. The Lower sandstone unit is characterized by submature quartzarenite, subarkose and arkose. The sandstones have been examined using scanning electron and hot-cathodoluminescence microscopy to study the albitized detrital feldspars. Detrital K-feldspar is the major feldspar that has been partly albitized throughout the study sandstone. The textural variation is considerable, including vein-like, blocky, and patchy forms. Probable sodium sources for albitization include smectite to illite or chlorite transition, diabase sills, detrital albite dissolution, and replacement of detrital sodium plagioclases by authigenic minerals. From comparison with other basins worldwide, a temperature estimate of 75–130°C for the mesodiagenetic albitization is inferred, suggesting a burial depth of 2000-5500 m based on a thermal burial model for the basin. The model suggests that the temperature at the base of the Padeha Formation did not exceed 150°C, constraining conditions for albitization.

Keywords: Alborz Mountain, Padeha Formation, Devonian, Albitization, Gondwana.

Introduction

The albitization of feldspar is a common diagenetic process that has been reported by many investigators in sandstones (Morad, 1988; Milliken, 2005; González-Acebrón et al., 2010; Poursoltani & Gibling, 2011; Poursoltani et al., 2019). As some investigators argued (Saigal et al., 1988; Morad et al., 1990, 2000), albitization of feldspars can alter the composition of sandstone to form diagenetic products, such as carbonate components and some clay minerals. Thus, the study of albitization is a fundamental factor for petrographic studies on sandstones and diagenetic stages (Poursoltani et al., 2019; Poursoltani & Pe-Piper, 2020). Additionally, the presence of albitization helps to interpret the provenance and burial depth of siliciclastic deposits (González-Acebrón et al., 2010; Taylor et al., 2010; Poursoltani & Pe-Piper, 2020; Poursoltani, 2021). As Morad et al., (1990) discussed, the albitization of feldspars usually requires a great burial depth.

The petrography and diagenesis of Devonian sandstones have received considerable study worldwide (e.g., De Ros, 1998; Avigad et al., 2005). The petrographic and diagenetic data presented provide insight into the depositional history, source exhumation, burial history and provenance of the sedimentary rocks. Provenance studies serve to reconstruct the predepositional history of a sediment or sedimentary rock. This includes the distance and direction, size and setting of the source region, climate and relief in the source area, the specific type of sedimentary rock (Pettijohn et al., 1987; McCann, 1998), and geochemical features

* Corresponding author e-mail: poursoltani1852@mshdiau.ac.ir

(Bhatia & Crook, 1986; Roser & Korsch, 1988; Armstrong-Altin et al., 2004; Hossam et al., 2011). Poursoltani & Pe-Piper (2020) documented the petrography and provenance of the Padeha Formation in the study area. They found that the sandstones were sourced from the widespread granitic gneisses of central and northern Iran that formed at the northern margin of Gondwana in the late Neoproterozoic–Ediacaran. Diagenesis of the sandstones is dominated by compaction and fracturing of framework quartz, and cementation by silica, carbonates and Fe-oxides. They also suggested that the principal source rocks were I-type granitoids, with minor metamorphic rocks, seen as lithic clasts. The sandstones were sourced from the widespread late Neoproterozoic granitic gneisses that formed juvenile crust at the northern margin of Gondwana.

The main purpose of the present study is to clarify albitization of detrital feldspars in the basal sandstone of the Padeha Formation in the Eastern Alborz. We present petrographic information concerning albitization for a large number of sandstone samples, based on scanning electron microscopy and hot-cathodoluminescence microscopy of polished thin sections, yielding insight into probable sodium sources.

Geological setting and stratigraphy

During the Paleozoic, Iran was located adjacent to the Afro–Arabian continental platform on the northern cratonic margin of Gondwana (Stöcklin, 1968; Ruban et al., 2007; Poursoltani & Pe-Piper, 2020; Fig.1). As several researchers argued (Berberian & King 1981, Alavi 1996; Lasemi 2001; Bagheri & Stamfli, 2008), in northern Iran, Middle-Ordovician to Devonian magmatism is interpreted as a rift-related event, and evolution of this rift led to the formation of Paleotethys Ocean along the modern site of Alborz Mountains. Volcanosedimentary deposits of the Upper Paleozoic (Devonian to Permian) were deposited in this basin, following a Silurian episode of intense rift volcanic activity, southward spreading of the Paleotethys rifting and subsidence along newly formed younger faults in the Early-Middle Devonian (Aharipour et al., 2010). A terrestrial syn-rift succession of Early Devonian age was followed by marine deposits (siliciclastic deposits of the Padeha Formation and carbonate deposits of the Khoshieylagh Formation), which extended across the Alborz, central Iran, and Zagros blocks (Berberian & King 1981). The Padeha strata underlie Middle or Upper Devonian marine strata (Koshieylagh Formation), and they generally have been regarded as Lower to Middle Devonian based on their stratigraphic position and palynological data (Alavi-Naini, 1993; Wendt et al., 2002, 2005), although other palynological studies have suggested a Late Devonian age (Ghavidel- Syooki, 1994; Ghavidel-Syooki & Owens, 2007).

The Alborz region is the northernmost geological-structural zone of the Iranian plateau (Stöcklin 1968) (Fig. 1A), trends east-west, and is sub-divided into western, central and eastern parts. The study area lies in the eastern Alborz Mountain (Fig. 1A). In Plemis area, Silurian rocks (Niur Formation) and Devonian rocks (Padeha and Khoshieylagh formations) are well exposed (Fig. 1B), and the base and top of the Padeha Formation are preserved, with the base disconformably overlying the Niur Formation. The Padeha Formation is overlain by the Khoshieylagh Formation, comparable to the succession in Central Iran. The thickness of the formation in the study area is 600 m. A basal unit of sandstone (hereafter referred to informally as the “lower sandstone”) is 115 m thick, and consists of thick beds of sandstone interbedded with thin beds of shale and siltstone and rarely very coarse conglomerate. The lower sandstone includes four basaltic sills with an aggregate thickness of 13 m, of unknown age (Figs. 2, 3).

The Padeha Formation in the Tabas Block was deposited in a tidal-flat environment (Zand-Moghadam et al., 2014), whereas the time-equivalent rocks in the Zagros and the Lut Block, as well as the Padeha Formation in the eastern Alborz, were deposited in a continental environment (Wendt et al., 2005; Aharipour et al., 2010). As Aharipour et al. (2010) discussed,

in the eastern Alborz the Padeha Formation was deposited in a terrestrial environment (alluvial fan, distal fan, and lake). They inferred that the lower sandstone of the Padeha Formation was deposited by processes of braided rivers in a proximal to medial alluvial fan. The lack of index fossils in the probable Lower Devonian successions hinders precise interpretation of paleogeography at this time.

Burial History

Burial history was assessed using the age and average thickness of the strata, not corrected for compaction, for the Pelmis area, between Shiroyeh and Sarinow faults, where a detailed map is available (Afshar-Harb et al., 1987) (Fig. 1B). The dataset was supplemented by regional evaluations of stratal relations and faults, with numerous regional tectonic episodes (Ruban et al., 2007).

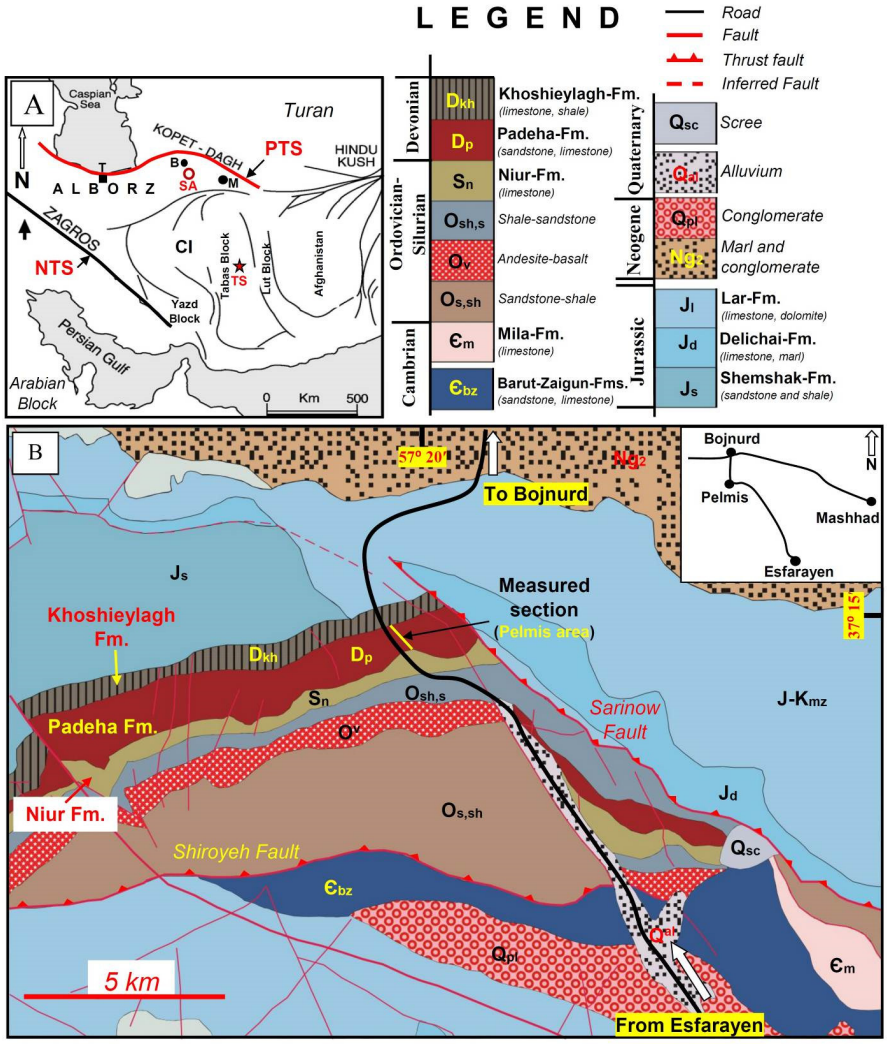

Figure 1. A) Location map of Iran and study area in the eastern Alborz, relative to plates and major tectonic zones. T: Teheran; M: Mashhad; B: Bojnurd; NTS: Neo-Tethys Suture; PTS: Paleo-tethys Suture; SA: study area; TS: type section of the Padeha Formation in the Central Iran; CI: Central Iran. Upper case names indicate major mountain belts. The arrow indicates present-day relative motions. Modified from Berberian & King (1981). B) Geological map showing the location of the studied section, simplified from Iran Geological Survey map sheet Bojnurd (1:250,000 scale) (Afshar-Hab, 1987)

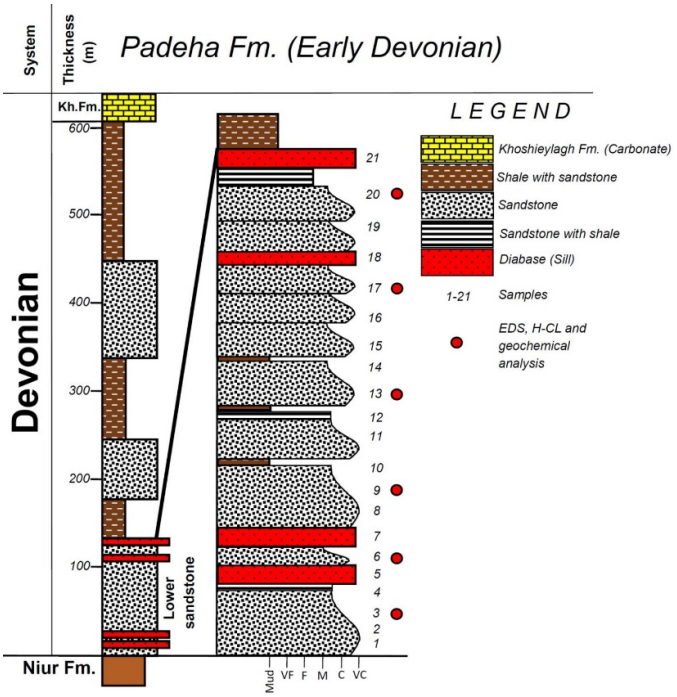

Figure 2. Stratigraphic log for the Padeha Formation in the study section, showing sample positions. Location of section is shown in figure 2B. Numbers show sample positions. Black numbers show samples for modal analysis, and red circles show samples with H-CL and EDS analysis. (vf: very fine; f: fine; m: medium; c: coarse; vc: very coarse)

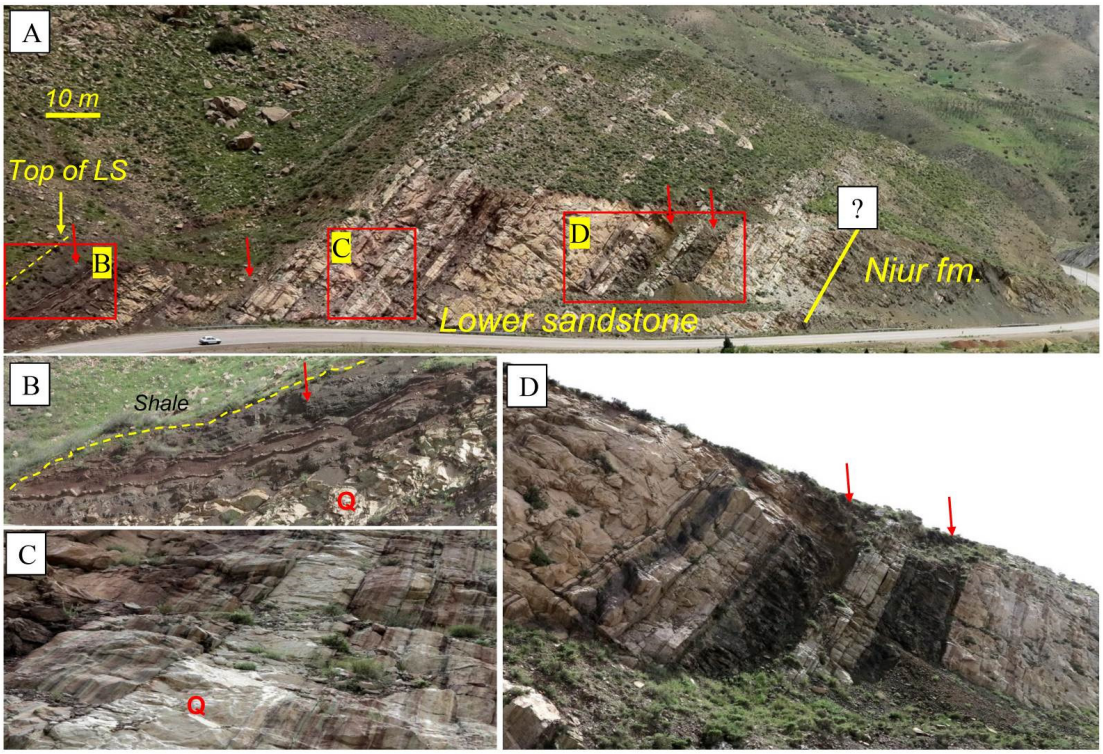

Figure 3. A) Field photos of the lower sandstone of the Padeha Formation in the Pelmis area, where it is ~115 m thick, including sills (red arrows). Yellow lines show formation and unit contacts B) upper contact of Lower sandstone unit; C, D) close up of quartoz bed sandstone and sills. (Q: quartzarenite; LS: lower sandstone)

There is considerable uncertainty about the thickness of strata eroded beneath the numerous mapped discontinuities. Hiatuses shown on Fig. 4 were accompanied by unconstrained but probably modest exhumation. The results are considered provisional in view of varied stratal thickness across the region, limited biostratigraphic information, regions of no exposure, and numerous faults.

In the Pelmis area, the aggregate thickness of the strata from the base of the Padeha Formation to the youngest Quaternary is ~5.5 km. In view of the numerous discontinuities, the aggregate thickness at the study area probably did not exceed 5 km (Fig. 4). Assuming a surface temperature of 25 °C and a geothermal gradient of 25 °C/km (Turcotte & Schubert, 2002), on the Gondwanan continental margin during the Paleozoic, the temperature at the base of the Padeha Formation may not have exceeded 150°C. However, the presence of sills suggests one or more periods with higher geothermal gradient, although their timing and duration is not known (Fig. 3).

Methods

The main stratigraphic section was logged graphically (Fig. 2), and 25 fresh sandstone samples were systematically collected, from which 21 thin sections were made (17 sedimentary, four igneous samples). Modal petrographic analyses were made on a Nikon Eclipse E400 Pol microscope with a Pixe Link PL-B623CU camera, and 400 points were counted in each thin section, from 17 sandstone samples, at Saint Mary's University, Canada, following the Gazzi-Dickinson method (Ingersoll et al., 1984), with counts of matrix and cement. Sandstones were classified following Folk (1980). Results are summarized in Table 1. Calculation of sorting followed the visual method of Friedman et al. (1992).

Table 1. Petrographic analysis of 17 samples from the lower sandstone of Padeha Formation, based on counting of 400 points for each sample. Table shows percentage of grains, and cement proportions. Counting followed the Gazzi-Dickinson method (Ingersoll et al., 1984). For grain counts, Qm: monocrystalline quartz; Qp: polycrystalline quartz; K-Feld: K-feldspar; Plag: Plagioclase; VRF, MRF and SRF: volcanic, metamorphic and sedimentary rock fragments; respectively; HM: heavy minerals. For maturity; Qt: total quartz; F: total feldspar; RF: total rock fragments

Sample Code	QUARTZ		FELDSPAR		ROCKFRAGMENT			A.M.	SUM	CEMENT				SUM
	Qm	Qp	K-Feld	Plag	VRF	MRF	SRF			SILICA	CARB.	CLAY	FE-OXIDE	
P1	59.54	12.76	21.62	5.08	0.00	0.00	0.00	1.00	100.00	49.47	31.80	0.00	18.73	100
P2	65.09	16.56	14.17	3.72	0.00	0.46	0.00	0.00	100.00	76.92	6.59	1.83	14.65	100
P3	64.44	15.84	12.15	5.57	0.00	0.00	0.00	2.00	100.00	92.86	0.00	7.14	0.00	100
P4	39.26	3.97	38.81	15.25	0.00	0.00	2.70	0.00	100.00	18.42	70.66	3.85	7.07	100
P6	68.44	12.81	15.31	3.44	0.00	0.00	0.00	0.00	100.00	58.33	25.00	0.00	16.67	100
P8	66.29	8.49	17.74	4.49	0.00	0.00	0.00	3.00	100.00	84.38	0.00	3.13	12.50	100
P9	65.20	10.19	19.54	4.07	0.00	0.00	0.00	1.00	100.00	100.00	0.00	0.00	0.00	100
P10	76.77	8.41	11.75	3.08	0.00	0.00	0.00	0.00	100.00	100.00	0.00	0.00	0.00	100
P11	35.55	10.27	33.57	20.18	0.00	0.44	0.00	0.00	100.00	83.13	0.00	3.29	13.58	100
P12	67.23	1.71	20.90	7.31	0.85	0.00	0.00	2.00	100.00	78.26	8.70	2.17	10.87	100
P13	47.65	12.79	26.72	3.90	6.42	0.53	0.00	2.00	100.00	11.31	31.86	0.00	56.82	100
P14	54.72	18.97	20.84	5.47	0.00	0.00	0.00	0.00	100.00	0.00	84.71	0.00	15.29	100
P15	46.05	18.11	22.95	11.89	0.00	0.00	0.00	1.00	100.00	62.50	0.00	0.00	37.50	100
P16	33.33	6.36	40.48	19.83	0.00	0.00	0.00	0.00	100.00	31.03	44.83	0.00	24.14	100
P17	59.49	8.33	22.59	5.00	1.21	1.14	2.24	0.00	100.00	0.00	73.81	0.00	26.19	100
P19	66.95	9.48	18.29	4.48	0.20	0.61	0.00	0.00	100.00	58.31	0.00	22.23	19.46	100
P20	57.96	5.92	21.97	6.44	0.79	2.51	1.41	3.00	100.00	72.16	15.19	0.00	12.65	100
AVERAGRE	**57.29**	**10.64**	**22.32**	**7.60**	**0.56**	**0.33**	**0.37**	**0.88**		**57.48**	**23.13**	**2.57**	**16.83**	

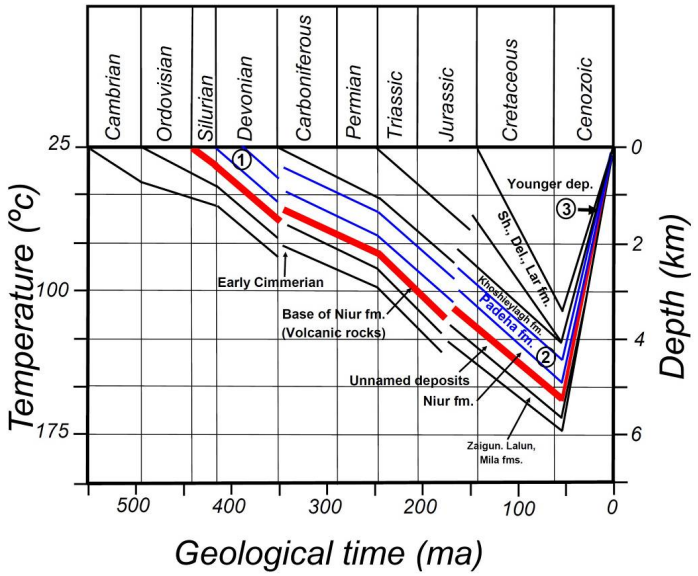

Figure 4. Burial diagram for the base of the Padeha Formation, based on stratigraphic age and thickness of strata (from Aghanabati, 2004) in the Pelmis area (Fig. 1B), eastern Alborz. The thermal history assumes a surface temperature of 25 °C and a geothermal gradient of 25 °C/km during the early period of basin subsidence. See text for discussion of uncertainties

The chemical composition of mineral components of six carbon-coated polished thin sections (sample numbers: 3-6-9-13-17-20) were determined by BSE, with particular emphasis on feldspars. The Scanning Electron Microscope (SEM) used at Saint Mary's University was a LEO 1450 VP at an acceleration voltage of 30.00 kV, equipped with an Oxford 80 mm^2 SDD–EDS detector and INCA software, operated in Backscattered Electron mode (SEM-BSE). Luminescence characteristics of the same sandstone suite were studied using a conventional hot-cathode luminescence (HCL) microscope (Lumic, model HC4-LM) with Kappa DX 40C cooled camera (cf., Neuser et al., 1995).

The operating conditions were 13-14 kV, 0.32 mA, and 12 dB, with a 6 second exposure. BSE and CL images used to investigate geochemical data were interpreted to constrain the diagenetic history and mineral paragenesis of the sandstones. Microanalytical tests were performed on 6 coated thin sections on the feldspar grains, and oxides (SiO2, Al2O3, Na2O, K2O, BaO, CaO, TiO2, MnO, MgO, FeO) and elements (Ca, Na, K, S) were measured. Results are summarized in Table 2.

Results

Petrography and provenance

The lower sandstone unit is characterized by fine- to coarse-grained, subangular to rounded grains. On average, most samples are well-sorted, with some moderately sorted and the remainder poorly to very well sorted, and rarely very poorly sorted (Fig. 5). Most sandstones are submature, whereas some are mature and rarely supermature (Folk, 1951). The mineral constituents are detrital quartz (monocrystalline, polycrystalline), K-feldspar (euhedral and anhedral), un-twinned orthoclase, plagioclase (mostly albite), rarely perthite feldspar, lithic clasts (volcanic, sedimentary, metamorphic clasts), heavy minerals (mostly zircon and rutile), and micas (Table 1). Most of the studied sandstones are characterized by their quartzofeldspathic nature, and are classified as quartzarenite, subarkose, and arkose (cf. Folk, 1980) (Fig. 5). The main cement is silica, with lesser abundance of carbonate, iron oxides, and clays (mostly chlorite) (Fig. 6).

Table 2. Results of geochemical analyzes of 52 points of 6 samples of lower sandstone of Padeha Formation by EDS method, normalized to 100%

Sample	Point	Mineral	SiO2	Al2O3	FeO	MnO	MgO	CaO	Na2O	K2O	P2O5	SO3	Cl	Cr2O3	ZnO	ZrO2	BaO	Total
Fig.10A																		
P3	1	K-feldspar	66.42	17.8					0.55	15.3								99.99
P3	2	Albite	68.88	18.8				0.07	11.5	0.76								99.99
P3	3	Pyrite	5.16	1.55	25.5			0.08		0.94		65.92				0.82		100.01
P3	4	Albite	68.75	19	0.12			0.29	11.6	0.26								100
P3	5	Dolomite	1.37		4.16	1.43	47.9	44.8		0.37								100.01
Fig.10B																		
P17	1	K-feldspar	65.84	18.1					1.12	14.9								100.02
P17	2	Chlorite	35.72	21.8	16.3		14.2	4.81		1.71	3.87	0.45			1.1			99.98
P17	3	K-feldspar	65.63	18.2					1.43	14.2							0.5	99.99
P17	4	K-feldspar	65.69	18					0.44	15.8								99.99
Fig.11C																		
P13	1	K-feldspar	65.63	17.8					0.24	16							0.4	100
P13	2	Albite	69.05	18.1	0.54				12	0.34								100.01
P13	3	Albite	68.97		18.9	0.14			0.08	11.9								100
P13	4	Albite	69.05	18.7					12.3									100
P13	5	Albite	65.61	18.1	0.27				10.3	5.72								99.99
Fig.12A																		
P3	1	K-feldspar	65.63		17.8					0.24	16						0.4	100
P3	2	Albite	68.84	17.6	0.33				12	1.14								99.98
P3	3	Albite	65.61		18.1	0.27				10.3	5.72							99.99
P3	4	K-feldspar	66.12	17.5						16.4								100.01
P3	5	Quartz	98.27	1.48		0.26												100.01
P3	6	K-feldspar	67.68	18.1	0.67			0.81	7.7	3.36	0.99			0.73				100
Fig.12B																		
P17	1	K-feldspar	65.74	18.1					1.55	14.1					0.5			100.01
P17	2	Albite	68.54	18.5					10.5	2.52								100.02
P17	3	Quartz	96.2	2.82						0.99								100.01
Fig.13A																		
P6	1	K-feldspar	66.1	17.6					0.4	15.9								99.98
P6	2	Albite	68.75	19					12.3									100
P6	3	K-feldspar	66.21	17.6					0.53	15.7								100.02
P6	4	Albite	69.14	18.7					12.2									100.02
P6	5	Dolomite			4.75	1.95	48.2	45.1										100.02
P6	6	K-feldspar	66.21	17.8						16								100.01
P6	7	Dolomite				4.55	2.09	47.4	46									99.99
Fig.13B																		
P20	*1*	K-feldspar	*66.12*	*18.2*					*1.23*	*14.4*								*99.99*
P20	*2*	*Albite*	*68.95*	*18.5*	*0.3*			*0.17*	*11.7*	*0.4*								*100.01*
P20	*3*	K-feldspar	*66.27*	*17.9*					*0.81*	*15*								*100*
P20	*4*	*Albite*	*68.2*	*18.5*					*10.3*	*3.05*								*100.01*
P20	*5*	*Quartz*	*99.99*															*99.99*
P20	*6*	K-feldspar	*66.25*	*18.1*					*7.63*	*8.03*								*99.97*
P20	*7*	Albite	69.05		18.1	0.54				12	0.34							100.01
Fig. 14A																		
P9	1	Albite	65.46	19.8	1.13			0.98	11.1	1.11	0.48							100.01
P9	2	Calcite			0.45	0.48	1.38	97.7										100.02
P9	3	Albite	67.53	19.2	0.77			0.29	11.5	0.66								99.99
P9	4	Calcite				0.41	0.71	98.9										99.99
P9	5	Albite	66.98	20.4				1.68	10.5	0.46								100.03
P9	6	K-feldspar	65.16	18.3	0.75		0.4		0.36	15.1								100
P9	7	K-feldspar	66.36	18					1.71	13.9								100
P9	8	Quartz	94.23		3.02						2.76							100.01
Fig.14B																		

P6	1	Quartz	99.58									0.41	99.99
P6	2	K-feldspar	66.49	18.1	0.49				0.78	13.6		0.51	99.99
P6	3	Albite	67.9	18.7					10	3.01		0.35	99.99
P6	4	K-feldspar	66.02		17.8					0.5	15.7		100.01
P6	5	K-feldspar	66.1		17.9					0.43	15.6		100.01
P6	6	Albite	68.09	18.8	0.33			0.31	11.2	0.86		0.39	100.01
P6	7	Calcite			0.41	0.58	0.99	98					99.99

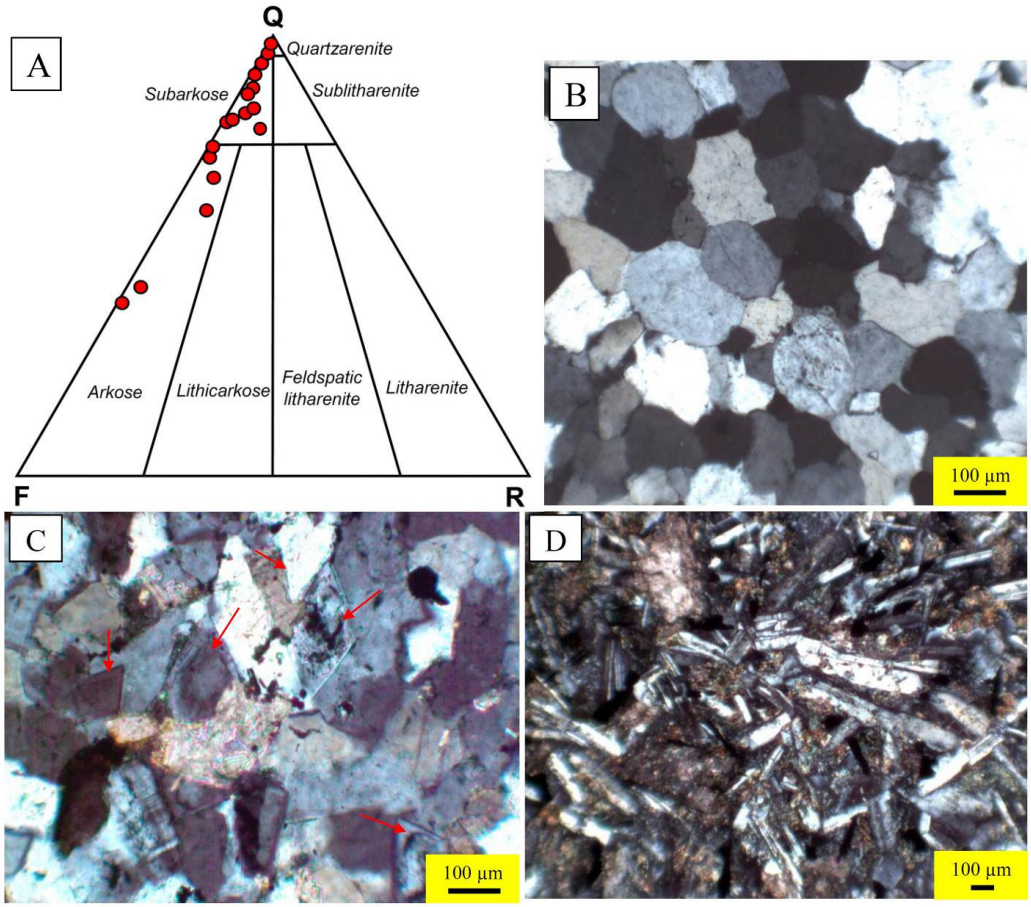

Figure 5. Composition and texture of 17 Padeha Formation sandstones. A) Quartz-Feldspar-Rock fragment triangle (Q-F-RF) (Folk, 1980). B) Supermature quartzarenite. C) Arkosic arenite; arrows showing euhedral feldspars. D) Diabasic igneous rock (from sills). Photographs taken under cross-polarized light

Based on the petrographic results, a paragenetic sequence is proposed for the sandstones, including three general stages of eogenesis, mesogenesis and telogenesis (Poursoltani and Pe-Piper, 2020). These authors also mentioned that Padeha Formation sandstones were deposited in an Early to Middle Devonian rift basin derived from plutonic with minor metamorphic rocks at the northern margin of Gondwana. Cementation, compaction and fracturing, pressure solution, K-feldspar overgrowths, and albitization were occured during mesogenesis. The base of the Padeha Formation achieved depths of burial from about 1400 and 5800 m from the end of the Carboniferous to the end of the Cretaceous, reaching a maximum temperature of approximately 150°C or less (Fig. 4). The albitization processes described in this research took place during the mesodiagenetic stage, when the maximum temperatures varied between about 75 and 150°C.

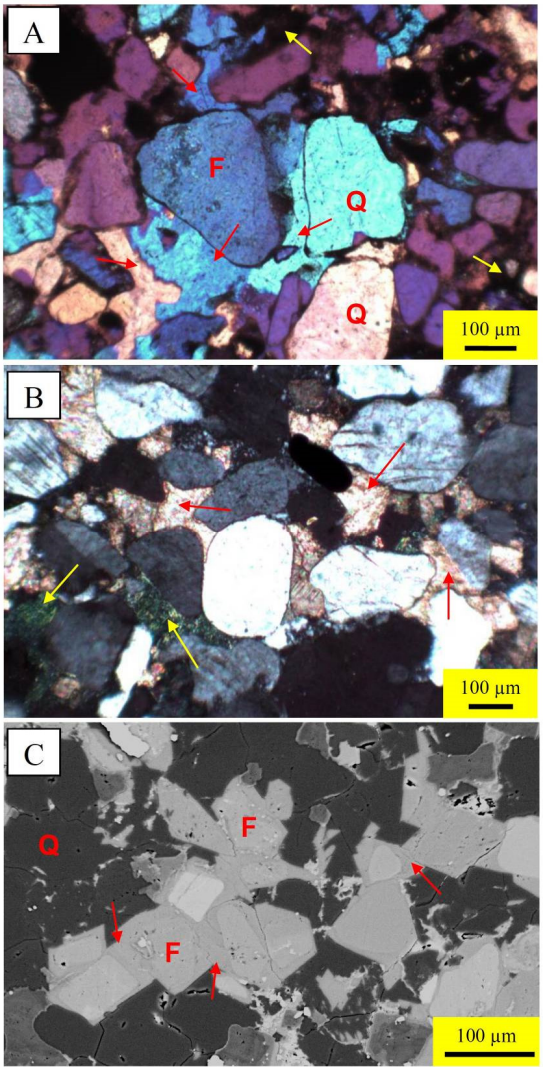

Figure 6. Type of main cements in Padeha Formation sandstones. A) Large area of silica cement (red arrows); yellow arrows show iron-oxide cement, using λ wedge. B) Carbonate pore-fills (red arrows), and glauconite pore-fills (yellow arrows), using XPL. C) Authigenic feldspar overgrowths (red arrows) around detrital feldspars; back-scattered electron photomicrograph (F: feldspar, Q: quartz)

Albitization of feldspar

Detrital K-feldspar is the major feldspar type that has been partly albitized throughout the lower sandstone of the Padeha Formation. Detrital perthites are generally fresh (Fig. 7C). The detrital K-feldspar is usually fresh or, rarely, slightly albitized or partially dissolved. BSE and Hot-CL images reveal that, irregularly, albite was partially replaced, in contrast to the alteration and dissolution of detrital K-feldspar, which took place mostly along cleavage planes and microfractures (Fig. 8).

Cathodoluminescence colors of unaltered feldspars are commonly bright blue and yellow-green to shades of brown, green and blue, while diagenetic albite displays dark luminescence color (Fig. 9B, E). Darker parts of albitized grains are strongly albitized areas, whereas the lighter parts are less sodium rich in BSE images (Fig. 8A).

The diagenetic albite is untwinned and displays patchy extinction patterns (Fig. 11) (Milliken, 2005). The albitized feldspars contain variable amounts of dissolution voids, which are filled by blocky diagenetic albite. Some of the dissolution voids are thought to have formed by leaching of

the feldspar grains during pre-albitization events, particularly in the early eogenetic regime (Fig. 9).

Some of the partially albitized plagioclase/K-feldspar grains contain variable amounts of dolomite and pyrite, indicating dissolution subsequent to overgrowth (Fig. 8A) (e.g. Morad et al. 1990). Albitization is most common at burial depths in the range of 2000 m to 5500 m (cf. Gold 1987; Saigal et al. 1988; Morad et al., 1990). In the lower sandstone unit, K-feldspar overgrowths are also prominent (Figs. 6C, 8B).

Scanning Electron Microscopy

Based on BSE results, considerable textural variation of the authigenic albite is present in the lower sandstone unit, including vein-like, blocky, and patchy forms (e.g., Boles 1982; Gold 1987; Milliken, 1989; González-Acebrón et al., 2010; Petersson et al., 2012). In the simplest case, both the albite and the authigenic K-feldspar precipitated as ordinary cements in spaces not formerly occupied by detrital grains, within microfractures (Fig. 9), as pore fills, and as overgrowths on the detrital feldspar grains.

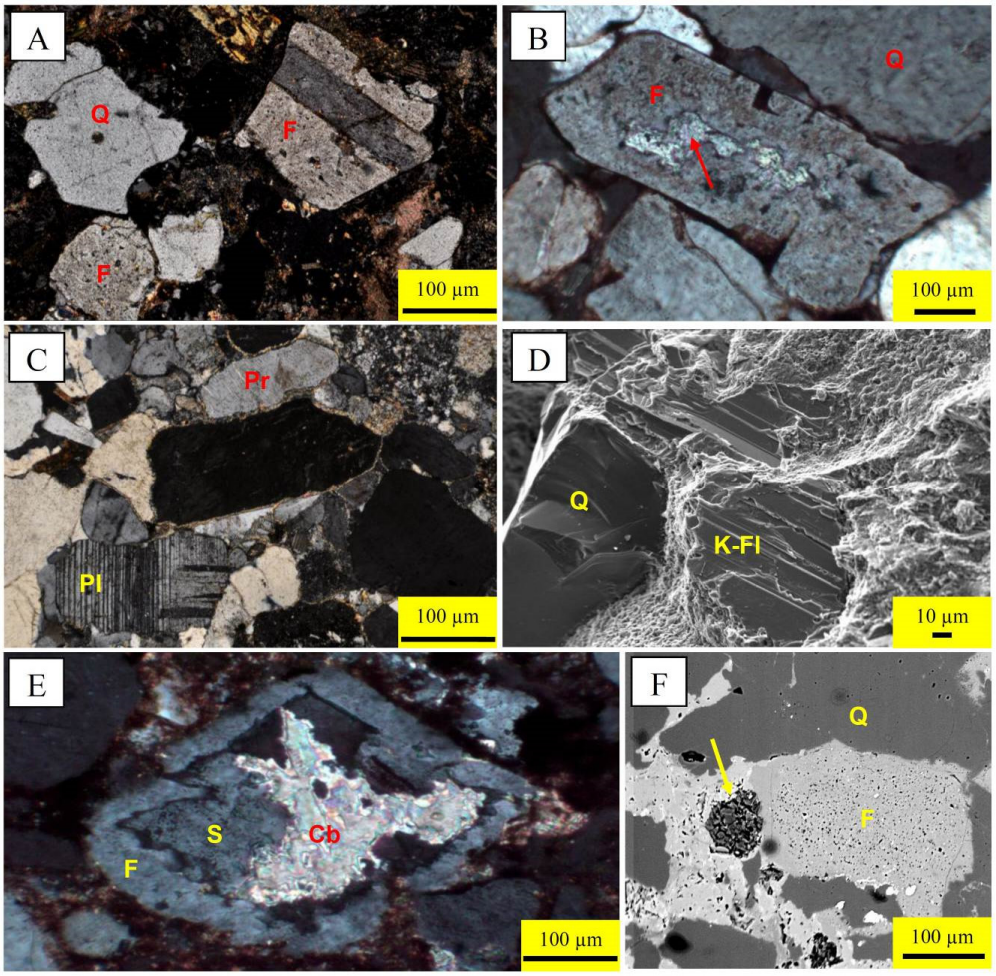

Figure 7. Photomicrographs of the different types of feldspars in the lower sandstone of the Padeha Formation in the Pelmis area. A) Twinned bright rectangular plagioclases riddled with fluid inclusions (XPL). B) Untwinned, turbid K-feldspars or plagioclases, with silica replacing feldspar (arrow) (XPL). C) Polysynthetic twinned plagioclase, and perthite in microcline or orthoclase (XPL). D) Quartz and K-feldspar, using SEM. E) Dissolution of feldspar and replacement with silica and carbonate (XPL). F) Kaolinite pore fills and replacing K-feldspar (arrow) (using BSE) (Q: quartz; F: feldspar; Pl: polysynthetic plagioclase; Pr: perthite; S: silica; Cb: carbonate)

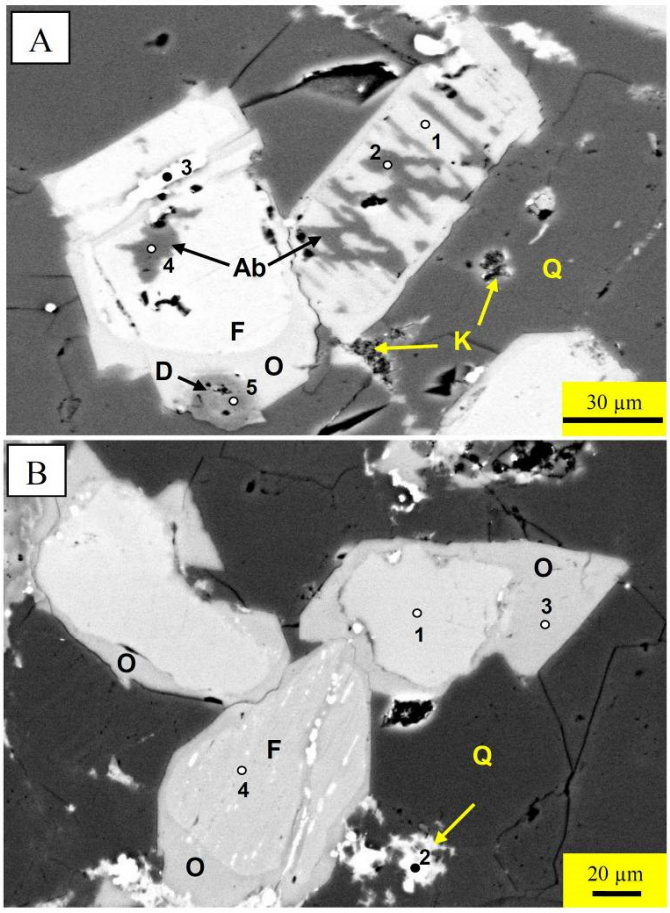

Sample	Point	Mineral	SiO2	Al2O3	FeO	MnO	MgO	CaO	Na2O	K2O
A										
P3	*1*	*K-feldspar*	*66.42*	*17.8*					*0.55*	*15.3*
P3	*2*	*Albite*	*68.88*	*18.8*				*0.07*	*11.5*	*0.76*
P3	*3*	*Pyrite*	*5.16*	*1.55*	*25.5*			*0.08*		*0.94*
P3	*4*	*Albite*	*68.75*	*19*	*0.12*			*0.29*	*11.6*	*0.26*
P3	*5*	*Dolomite*	*1.37*		*4.16*	*1.43*	*47.9*	*44.8*		*0.37*
B										
P17	*1*	*K-feldspar*	*65.84*	*18.1*					*1.12*	*14.9*
P17	*2*	*Chlorite*	*35.72*	*21.8*	*16.3*		*14.2*	*4.81*		*1.71*
P17	*3*	*K-feldspar*	*65.63*	*18.2*					*1.43*	*14.2*
P17	*4*	*K-feldspar*	*65.69*	*18*					*0.44*	*15.8*

Figure 8. Authigenic minerals involving feldspar in lower sandstones of Padeha Formation. A) Albitization in K-feldspars (black arrows), yellow arrows show kaolinite inside quartz grain. B) Authigenic feldspar overgrowths (O) around detrital feldspars; yellow arrows show chlorite pore-filling. (Back-Scattered Electron photomicrographs) (Q: quartz; F: feldspars; O: overgrowth; Ab: albite; D: dolomite). Numbers on the photos show the EDS analysis points, linked to geochemical results in the table below, normalized to 100%

The mechanism of albitization is probably a dissolution and precipitation process (Boles, 1982; Morad, 1988; Saigal et al., 1988; Ramseyer et al., 1992; Milliken & Olson, 2017). The textural evidence presented in this study shows that albitization is guided by weakness planes that include grain fractures, cleavage traces, and twinning planes (Figs. 9, 12B). The dissolution rate of feldspars is known to be greater at such planes due to their excess surface energy. These weak zones are conduits for the penetration of thin water films (Morad et al., 1990; Tawfik et al., 2011).

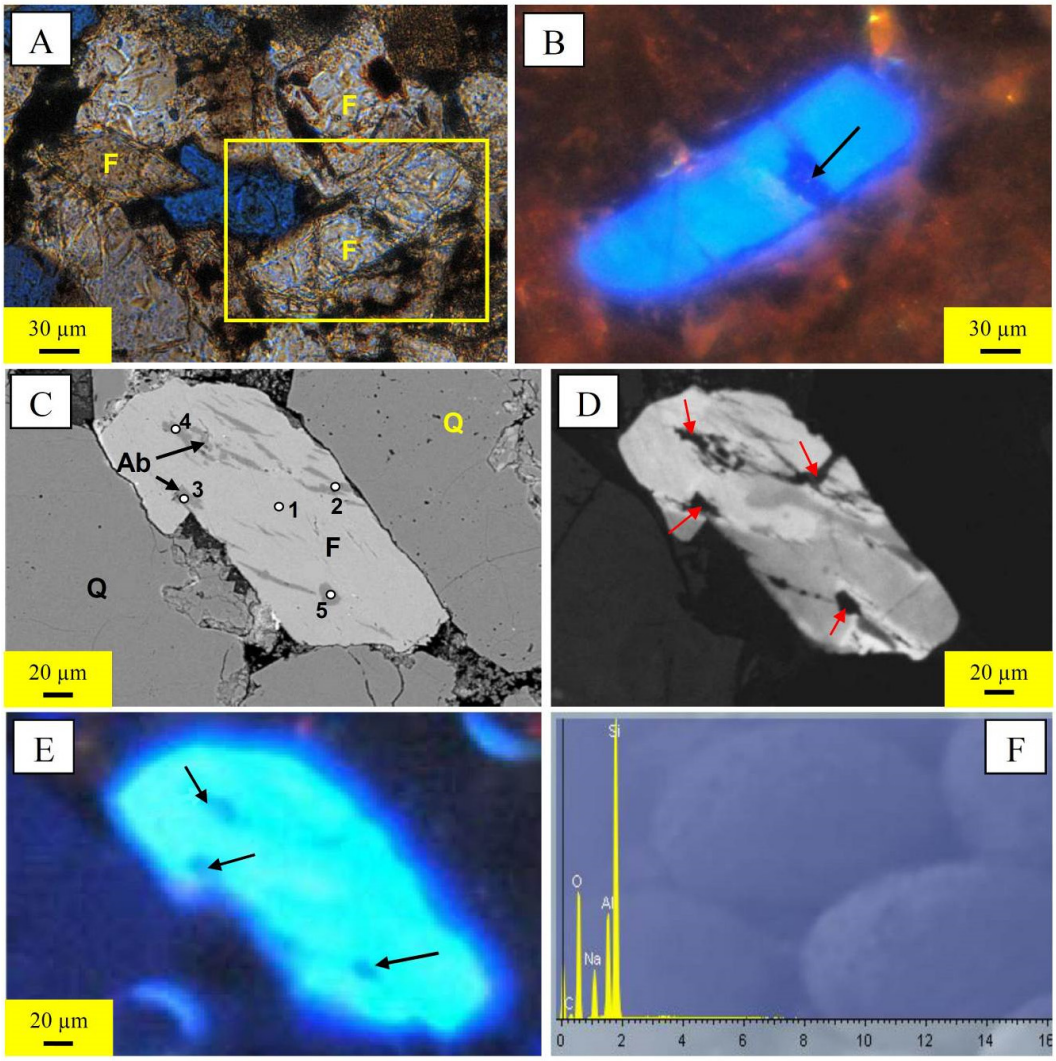

Sample	Point	Mineral	SiO2	Al2O3	FeO	MnO	MgO	CaO	Na2O	K2O
P13	*1*	*K-feldspar*	*65.63*	*17.8*					*0.24*	*16*
P13	*2*	*Albite*	*69.05*	*18.1*	*0.54*				*12*	*0.34*
P13	*3*	*Albite*	*68.97*		*18.9*	*0.14*			*0.08*	*11.9*
P13	*4*	*Albite*	*69.05*	*18.7*					*12.3*	
P13	*5*	*Albite*	*65.61*	*18.1*	*0.27*				*10.3*	*5.72*

Figure 9. Albitization of fractured feldspars. Fresh grains show intense blue luminescence, but albitized feldspar is almost non-luminescent (dark). A) View in crossed nicols. B) Panorama of A, showing the fractured feldspar. Arrow shows authigenic albite that fills the fracture. C) BSE image showing partially albitized feldspar grain. D) SEM-CL image of C, arrows showing the fractures. E) Cathodoluminescence image of C, arrows showing authigenic albite filling the fractures in the feldspar grain. F) Graph showing EDS analysis of authigenic albite. Numbers on the photos showing the EDS analysis points, and table shows the EDS analyses, normalized to 100%

Vein-filling authigenic albite precipitated in space formerly occupied by detrital feldspar displays variable degrees of replacement (Fig. 10A). This type of albite is associated with only minor development of secondary pores in the replaced grain.

Albite precipitated within grains has a "blocky" distribution, occurring in samples with a high degree of grain replacement. Commonly, dissolution occurred before albitization. Grains with domains of clear albite typically develop substantial secondary pores. Blocky domains of clear albite occur in K-feldspar (Fig. 10B). Another form of albitization is patchy, which was identified within detrital K-feldspars (Fig. 11A) and seems to occur as a post-dissolution process. Some samples show the marginal type of albitization, formed among clusters of grains or along the margins of individual grains (Fig. 11B). Authigenic K-feldspar is an early-formed phase, preceding most other common cementing minerals including calcite and quartz (Fig. 12).

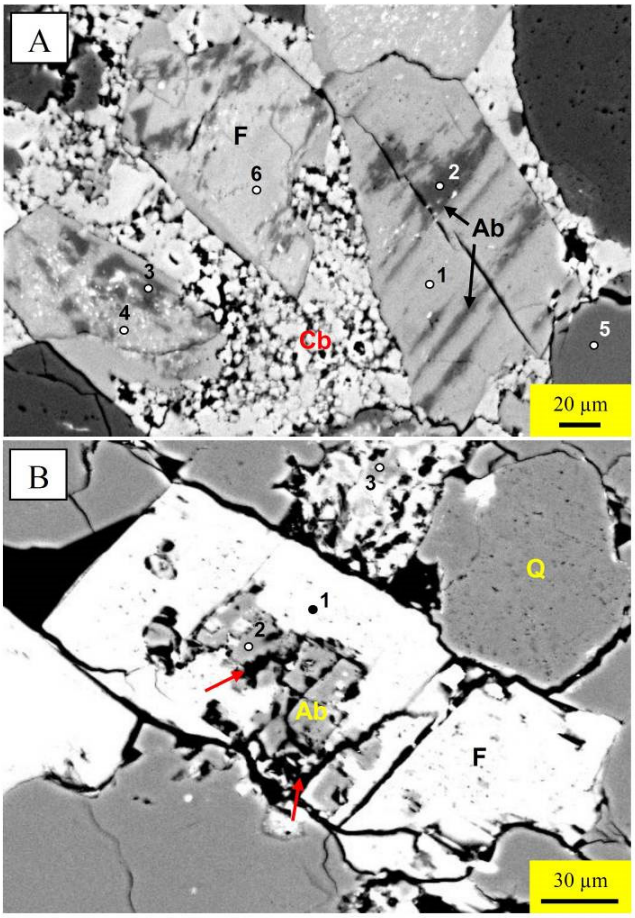

Sample	Point	Mineral	SiO2	Al2O3	FeO	MnO	MgO	CaO	Na2O	K2O
A										
P3	*1*	*K-feldspar*	*65.63*		*17.8*					*0.24*
P3	*2*	*Albite*	*68.84*	*17.6*	*0.33*				*12*	*1.14*
P3	*3*	*Albite*	*65.61*		*18.1*	*0.27*				*10.3*
P3	*4*	*K-feldspar*	*66.12*	*17.5*						*16.4*
P3	*5*	*Quartz*	*98.27*	*1.48*		*0.26*				
P3	*6*	*K-feldspar*	*67.68*	*18.1*	*0.67*			*0.81*	*7.7*	*3.36*
B										
P17	*1*	*K-feldspar*	*65.74*	*18.1*					*1.55*	*14.1*
P17	*2*	*Albite*	*68.54*	*18.5*					*10.5*	*2.52*
P17	*3*	*Quartz*	*96.2*	*2.82*						*0.99*

Figure 10. Back-scattered electron image of albitized feldspar grains. A) Replacement albite along the cleavages (arrows). B) Blocky authigenic albite. Arrows show pores, probable secondary porosity. (Ab: albite; F: feldspar; Q: quartz; Cb: carbonate). Numbers on the photos show the EDS analysis points, and the table shows the chemical composition expressed in percentages

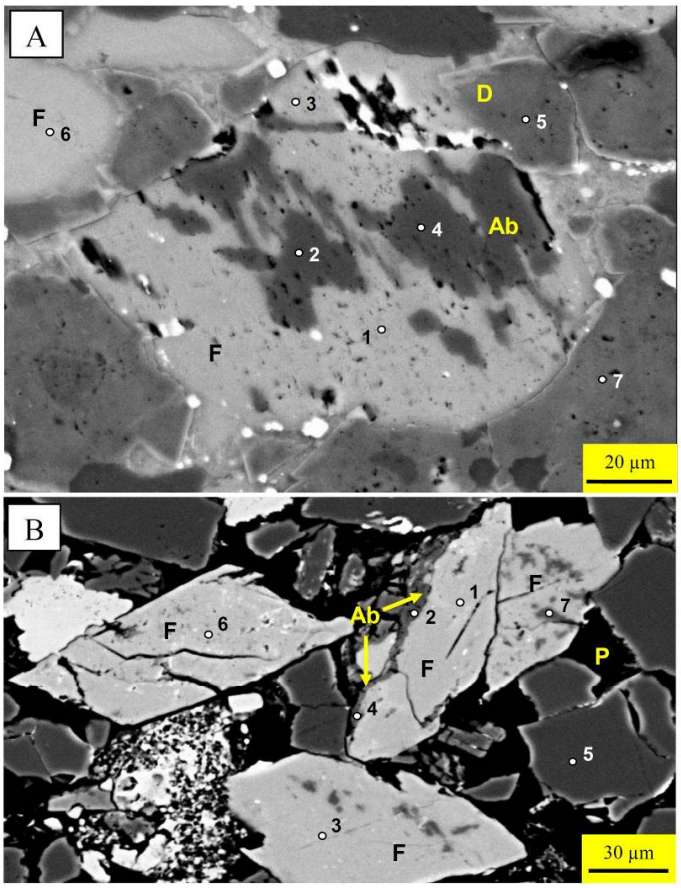

Sample	Point	Mineral	SiO2	Al2O3	FeO	MnO	MgO	CaO	Na2O	K2O
A										
P6	*1*	*K-feldspar*	*66.1*	*17.6*					*0.4*	*15.9*
P6	*2*	*Albite*	*68.75*	*19*					*12.3*	
P6	*3*	*K-feldspar*	*66.21*	*17.6*					*0.53*	*15.7*
P6	*4*	*Albite*	*69.14*	*18.7*					*12.2*	
P6	*5*	*Dolomite*			*4.75*	*1.95*	*48.2*	*45.1*		
P6	*6*	*K-feldspar*	*66.21*	*17.8*						*16*
P6	*7*	*Dolomite*				*4.55*	*2.09*	*47.4*	*46*	
B										
P20	*1*	*K-feldspar*	*66.12*	*18.2*					*1.23*	*14.4*
P20	*2*	*Albite*	*68.95*	*18.5*	*0.3*			*0.17*	*11.7*	*0.4*
P20	*3*	*K-feldspar*	*66.27*	*17.9*					*0.81*	*15*
P20	*4*	*Albite*	*68.2*	*18.5*					*10.3*	*3.05*
P20	*5*	*Quartz*	*99.99*							
P20	*6*	*K-feldspar*	*66.25*	*18.1*					*7.63*	*8.03*
P20	*7*	*Albite*	*69.05*		*18.1*	*0.54*				*12*

Figure 11. Types of albitization in the lower sandstone. A) Patchy type, replacement of authigenic albite within K-feldspar. Authigenic dolomite is also shown. B) Marginal type, authigenic albite took place along the margin of feldspar grains (yellow arrows). The secondary porosity is shown. (Ab: albite; F: K-feldspar; P: pore; D: dolomite). Numbers on the photos show the EDS analysis points, and table shows the EDS analyses, normalized to 100%

Source of sodium

Four probable sodium sources required for albitization of feldspars in the lower sandstone unit are identified as follows:

1- The interbedded shales probably contain both potassium sinks and sodium sources, thus, transitions from sodium-bearing smectite to illite or chlorite during burial (Poursoltani & Pe-Piper, 2020) could also have released Na+ cations (e.g., Morad et al. 1990; Barrenechea et al., 2001; Petersson et al., 2012).

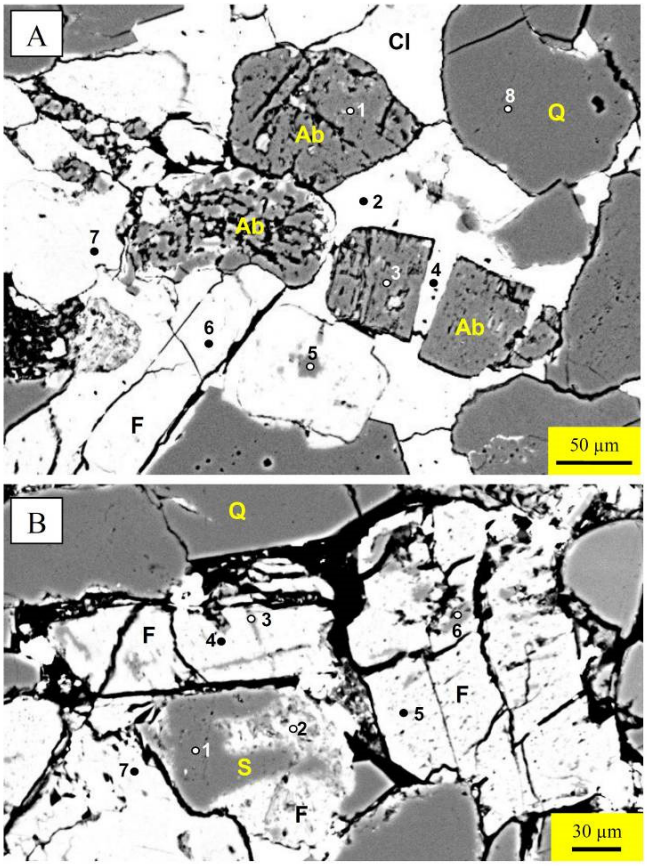

Sample	Point	Mineral	SiO2	Al2O3	FeO	MnO	MgO	CaO	Na2O	K2O
A										
P9	*1*	*Albite*	*65.46*	*19.8*	*1.13*			*0.98*	*11.1*	*1.11*
P9	*2*	*Calcite*			*0.45*	*0.48*	*1.38*	*97.7*		
P9	*3*	*Albite*	*67.53*	*19.2*	*0.77*			*0.29*	*11.5*	*0.66*
P9	*4*	*Calcite*				*0.41*	*0.71*	*98.9*		
P9	*5*	*Albite*	*66.98*	*20.4*				*1.68*	*10.5*	*0.46*
P9	*6*	*K-feldspar*	*65.16*	*18.3*	*0.75*		*0.4*		*0.36*	*15.1*
P9	*7*	*K-feldspar*	*66.36*	*18*					*1.71*	*13.9*
P9	*8*	*Quartz*	*94.23*		*3.02*					
B										
P6	*1*	*Quartz*	*99.58*							
P6	*2*	*K-feldspar*	*66.49*	*18.1*	*0.49*				*0.78*	*13.6*
P6	*3*	*Albite*	*67.9*	*18.7*					*10*	*3.01*
P6	*4*	*K-feldspar*	*66.02*		*17.8*					*0.5*
P6	*5*	*K-feldspar*	*66.1*		*17.9*					*0.43*
P6	*6*	*Albite*	*68.09*	*18.8*	*0.33*			*0.31*	*11.2*	*0.86*
P6	*7*	*Calcite*			*0.41*	*0.58*	*0.99*	*98*		

Figure 12. BSE images of the lower sandstones showing albitization and silicification. A) Partially dissolved albite grains, with authigenic albite replacing K-feldspar grains (point 5). B) Replacement of feldspar by silica (point 1) and albite along the cleavage (point 3). In both samples, carbonate is the main cement. (S: silica; F: feldspar; Ab: albite; Q: quartz; Cl: calcite). Numbers on the photos show the EDS analysis points, and table shows the EDS analyses, normalized to 100%

2- Sodium is a mobile element and may have been released from alteration of the associated diabase sills intercalated in the lower sandstone unit of the Padeha Formation (Fig. 3). Their alteration might be an additional source of Na for albitization (González-Acebrón et al., 2010; Poursoltani, 2021).
3- The lower sandstone is rich in detrital feldspars that include albite. Thus, dissolution of detrital albite grains could have released Na+ cations to contribute to authigenic albite formation elsewhere in the sandstone body and at a later time (Fig. 12A).
4-The replacement of detrital sodium plagioclases by authigenic minerals such as carbonate and silica can be another complementary source of sodium (Morad et al., 1990; Min et al., 2019) (Figs. 7F, 12B).

Discussion

Factors affecting the extent of albitization include a high rate of Na+ precipitation, temperature, formation water chemistry, porosity and permeability (Petersson et al., 2012; González-Acebrón et al., 2010).

High abundance of albite in a sandstone may indicate albitization, although albite can be detrital. Detrital albites can be derived from metamorphic or igneous rocks that have been altered prior to erosion by hydrothermal and post-magmatic processes. The timing and relative rates of dissolution and replacement determine the degree to which intergranular pores develop prior to, during, or after the precipitation process (Min et al., 2019). K-feldspar shares many features with albite, including vein-like distribution within detrital grains, compositional anomalies, and petrographic evidence of instability (Norberg et al., 2011).

Albitization may occur by direct replacement of feldspars by albite, or through intermediate stages that involve initial replacement of feldspars by authigenic minerals, followed by replacement of these minerals by albite (Walker, 1984). Albitization may also occur by partial dissolution of detrital feldspars, followed by precipitation of albite in dissolution voids (Milliken, 1989, Dutton & Loucks, 2010; Min et al., 2019). Albitization is revealed by the presence of distinctive textures in feldspars in the lower sandstones of Padeha Formation.

Authigenic albite is reported by several authors to occur at different temperatures. Several researchers (Milliken et al, 1981; Milliken 2003; Min et al., 2019) reported albitization temperatures of 100°-150° C, but albitization has also been reported to take place at lower temperatures on the order of 60°-100° C (Morad et al., 1990; Aagaard et al., 1990; Milliken et al., 2016). Morad et al. (1990) suggested that temperature is an important factor that accounts for the degree of albitization. In the Norwegian Triassic rocks, albitization of plagioclase occurred at temperatures of 75°—100° C. Also, Morad et al. (1990) suggested that albitization of K-feldspars would increase at greater burial depths and higher temperatures (>~125° C). In the Gulf of Mexico basin, dissolution of plagioclase took place at about 100-130°C, and plagioclase is replaced by albite in a similar temperature range, continuing to higher temperatures (Gold, 1987). Lower temperatures of 65-105°C for albitization were reported by Saigal et al. (1988) for North Sea reservoirs. As Boggs & Seyedolali (1992) reported, a temperature of 100° C is within the range at which albitization of plagioclase could be expected, assuming that permeability is adequate to promote fluid flow.

Total dissolution of K-feldspar has been documented at depths corresponding to temperatures ranging from 90 to 160°C, but mainly above 120°C (Boles & Franks, 1979; Milliken, 1989; Fisher & Land, 1986; see compilation in Gold, 1987; Milliken et al., 2016; Min et al., 2019; Poursoltani, 2021).

At the time of albitization of the lower sandstone of the Padeha Formation, temperature was likely much higher owing to the intrusion of basaltic sills into the sandstones. However, in several beds, the weak albitization of K-feldspars suggests that temperatures probably did not exceed

125° C. As mentioned, we cannot exclude the possibility that some of the albite grains in the lower sandstone are detrital feldspars that were derived by weathering of metamorphic rocks or igneous rocks, containing albite formed by hydrothermal and post-magmatic replacement of feldspars (e.g., AlDahan et al., 1987; González-Acebrón et al., 2010). Relatively low-temperature, early diagenetic or hydrothermal K-feldspar replacement of feldspars has been described in several volcanogenic sandstones (Aagaard et al., 1990; Milliken 2003; Min et al., 2019).

Diagenetic albitization would be expected since the albitization of K-feldspar is more likely at greater depths and temperatures (Morad et al., 1990). As González-Acebrón et al. (2010) mentioned, minimum entrapment temperatures of the albitization fluid are 83– 115 °C.

Based on above discussion, assuming a geothermal gradient of 25°C/km, a temperature of 75–130°C suggests a burial depth of 2000-5500 m for feldspar albitization in the lower sandstone unit of Padeha Formation. Thus, we interpret albitization as a mesodiagenetic burial process for the Padeha sandstones.

Other diagenetic processes that are relevant to albitization are the release of carbonate, kaolinite replacement (Poursoltani & Pe-Piper, 2020), and K-feldspar overgrowth. Calcium released by the albitization process may have increased the calcium content of ancient pore waters. Some calcium reprecipitated as calcite (or dolomite) that replaces framework grains and matrix in the lower sandstone (Fig. 7E). The carbonates that occur in the lower sandstone may be by-products of albitization (e.g., Boles, 1982; Milliken, 2003; Poursoltani; 2021). Calcite cements and replacements corrode albite overgrowths that precipitated in the immediate vicinity of albitized plagioclase grains, and they could thus be a by-product of calcic plagioclase albitization.

K-feldspar overgrowths are interpreted as eodiagenetic in origin (González-Acebrón, 2010), but some researchers have interpreted them as a mesodiagenetic process (Poursoltani et al., 2019; Milliken et al., 2016; Min et al., 2019). Albitization of K-feldspar overgrowths over detrital K-feldspar may have been simultaneous with albite cement formation over detrital plagioclases.

Albitization took place after the eodiagenetic K-feldspar cements, pointing again to a mesodiagenetic process (Dutton & Loucks, 2010; Poursoltani & Gibling, 2011; Poursoltani & Pe-Piper, 2020). The carbonates and kaolinite that occur in the lower sandstone may be by-products of albitization (e.g., Boles, 1982; Petersson et al., 2012; Min et al., 2019). Kaolinite is common only locally near the base of the formation, as pore fills and as replacements of K-feldspar in arkosic arenites, probably related to exhumation (Fig. 7F). Kaolinite pore fills and replacement of feldspar grains probably took place during deeper burial (González-Acebrón et al., 2010; Poursoltani et al., 2019). In many sandstones, this is the only occurrence mode of calcite and kaolinite, supporting their genetic relationship with the albitization. Precipitation of kaolinite from pore fluids late in diagenesis at temperatures of about 100°C or greater has been reported by several authors (e.g., Franks & Forester 1984; Fisher & Land 1986; Min et al., 2019). In summary, based on the above discussion and the burial history of the Padeha Formation, albitization is a mesodiagenetic process, and the temperature of albitization is inferred to have been about 100-130°C.

Conclusion

Albitization is prominent in the basal, terrestrial and arkosic sandstones of the Devonian Padeha Formation in the Eastern Alborz area of Iran. Based on BSE results, considerable textural variation of the authigenic albite is present in the lower sandstone unit, including vein-like, blocky, and patchy forms. Assuming a surface temperature of 25°C and a geothermal gradient of 25°C/km, the temperature at the base of the Padeha Formation may have been about 150°C during deepest burial in the earliest Cenozoic, providing an upper limit for the temperature associated with albitization. However, the presence of sills suggests one or more periods with higher geothermal gradient, although their timing and duration is not known.

Four probable sodium sources are identified: transitions from sodium-bearing smectite to illite or chlorite; alteration of four associated diabase sills; detrital albite dissolution; and replacement of detrital sodium plagioclases by authigenic minerals such as carbonate and silica.

Assuming a geothermal gradient of 25°C/km, a temperature range of 75–130°C (based on comparison with other sites worldwide) suggests a burial depth of 2000-5500 m for albitization of feldspars, based on an Early to Middle Devonian age for the formation. Thus, we interpret albitization as a mesogenetic burial process for the Padeha Formation sandstones.

Acknowledgment

The author thanks the Islamic Azad University of Mashhad, Iran, for financial assistance (number 99-R-70-25742), and anonymous reviewers for comments on an earlier manuscript version. He also thanks Prof. Martin R. Gibling of Dalhousie University, Canada, for reviewing the earlier draft, and also would like to thank technical staff at St. Mary's University, Canada, for assistance with the analyses.

References

Aagaard, P., Egeberg, P.K., Saigal, G.C., Morad, S., Bjorlykke, K., 1990. Diagenetic albitization of detrital K-feldspar in Jurassic, Lower Cretaceous and Tertiary clastic reservoir rocks from offshore Norway. II. Formation water chemistry and kinetic considerations. Journal of Sedimentary Petrology 60: 575-581.

Afshar-Hab, A., 1987. Geologic Map of Bojnurd, Geological Survey of Iran, Scale 1: 250000

Aghanabati, A., 2004. Geology of Iran. Geological Survey of Iran, 558 pp (in Persian).

Aharipour, R., Moussavi, M.R., Mosaddegh, H., Mistiaen, B., 2010. Facies features and paleoenvironmental reconstruction of the Early to Middle Devonian syn-rift volcano- sedimentary succession (Padeha Formation) in the Eastern-Alborz Mountains, NE Iran. Facies 56: 279-294.

Alavi, M., 1996. Tectonostratigraphic synthesis and structural style of the Alborz Mountains system in northern Iran. J Geodyn 21: 1-33.

Alavi-Naini, M., 1993. Paleozoic stratigraphy of Iran. Geology Survey of Iran, Treatise on the Geology of Iran 5, 492 pp. (in Persian).

AlDahan, A.A., Morad, S., Collini, B., 1987. Clouded-untwinned albite in the Siljan granite, central Sweden. N. Jahrb. Mineral. Monatsh., 1987: 327-335.

Armstrong-Altrin, J.S., Lee, Y., Verma, S.P. Ramasamy, S. 2004. Geochemistry of sandstones from the Upper Miocene Kudankulam Formation, Southern India: Implications for provenance, weathering and tectonic setting. J. Sedment. Res., 74: 285-297.

Avigad, D., Sandler, A., Kolodner, K., Stern, R.J., McWilliams, M., Miller, N. Beyth, M., 2005. Mass-production of Cambro-Ordovician quartz-rich sandstone as a consequence of chemical weathering of Pan-African terranes: Environmental implications. Earth and Planetary Science Letters 240: 818-826.

Bagheri, S., Stampli, G.M., 2008. The Anarak, Jandaq and Posht-e-Badam metamorphic complexes in central Iran: New geological data, relationships and tectonic implications. Tectonophisics, 451: 123-155.

Barrenechea, F.J., Rodas, M., Frey, M., Mas, J.R., 2001. Clay diagenesis and low-grade metamorphism of Tithonian and Berriasian sediments in the Cameros Basin (Spain). Clay Minerals 36: 325-333.

Berberian, M., King, G.C.P. 1981. Toward a paleogeography and tectonic evolution of Iran. Canadian Journal Earth Sciences, 18: 210- 265.

Bhatia, M.R., Crook, K.W. 1986. Trace element characteristics of greywackes and tectonic setting discrimination of sedimentary basins. Contributions to Mineralogy and Petrology 92: 181-193.

Boles, J.R., Coombs, D.S., 1977. Zeolite facies alteration of sandstones in the southland Syncline, New Zealand: Am. Jour. Science, 277: 982-1012.

Boles, J.R., Franks, S.G., 1979. Clay diagenesis in Wilcox sandstone of southwest Texas: implications of smectite diagenesis on sandstone cementation. Journal of Sedimentary Petrology 49: 55-70.

Boles, J.R., 1982. Albitization of plagioclase, Gulf Coast Tertiary. Am. J. Sci., 282: 165-180.

Boggs, S.Jr., Seyedolali, A., 1992. Diagenetic albitization, zeolitization, and replacement in miocene sandstones, sites 796, 797, and 799, Japan sea. In: Pisciotto, K.A., Ingle, J. C,Jr., von Breymann, M.T., Barron, J., et al., (Eds.), Proceedings of the Ocean Drilling Program, Scientific Results, 127/128, Pt. 1.

De Ros, L.F., 1998. Heterogeneous generation and evolution of diagenetic quartzarenites in the Silurian-Devonian Fumas Formation of the Paran Basin, southern Brazil. Sedimentary Geology 116: 99-128.

Dutton, S.P., Loucks, R.G., 2010. Diagenetic controls on evolution of porosity and permeability in lower Tertiary Wilcox sandstones from shallow to ultradeep (200-6700 m) burial, Gulf of Mexico basin, USA. Mar. Pet. Geol. 27: 69-81.

Fisher, R.S., Land, L.S., 1986. Diagenetic history of Eocene Wilcox sandstones, South-Central Texas. Geochimica Cosmochimica Acta 50: 551-561.

Folk, R.L., 1980. Petrology of Sedimentary Rocks. Hemphill Publishing, Austin, Texas, USA, 184 pp.

Franks, S.G., Forester, R.W., 1984. Relationships among secondary porosity, pore-fluid chemistry and carbon dioxide, Texas Gulf Coast, in McDonald, D., and Surdam, R., eeds., Clastic Diagenesis: Am. Assoc. Petroleum Geologists Mere. 37: 63-79.

Gazzi, P., 1966, Learenariedelfly schsopracretaceodell' Appenninomodenese; correlazioni con ilflysch di Monghidoro: Mineralogy Petrography Acta., 12: 69-97.

Ghavidel-Syooki, M., 1994. Biostratigraphy and paleo-biogeography of somePaleozoic rocks at Zagros and Alborz Mountains, Iran. Geology SurveyPublication, Iran, 168 pp.

Ghavidel-Syooki, M., Owens, B., 2007. Palynostratigraphy and paleogeographyof the Padeha, Khoshyeilagh and Mobarak formations in the eastern AlborzRange (Kopeh-Dagh region), northeastern Iran. Revue de Micropaleontol-ogy 50: 129-144.

Gold, P.B., 1987. Textures and geochemistry of authigenic albite from Miocene sandstones, Louisiana Gulf Coast. Journal of Sedimentary Petrology 57: 353-362.

González-Acebrón, L., Arribas, J., Ramón Mas, R., 2010. Role of sandstone provenance in the diagenetic albitization of feldspars A case study of the Jurassic Tera Group sandstones (Cameros Basin, NE Spain), Sedimentary Geology 229: 53-63.

Lasemi, Y., 2001. Facies analysis, depositional environments and sequence stratigraphy of the Upper Pre-Cambrian and Paleozoic rocks of Iran (in Persian). Iran Geol Surv Publ, pp. 1-180.

McCann, T. 1998. Sandstone composition and provenance of the Rotliegend and NE German Basin. Sediment. Geol. 116: 177-198.

Milliken, K.L., Land, L.S., Loucks, R.G., 1981. History of burial diagenesis determined from isotopic geochemistry, Frio Formation, Brazoria County, Texas. AAPG Bull, 65: 1397-1413.

Milliken, K.L., 1989. Petrography and composition of authigenic feldspars, Oligocene Frio Formation, South Texas. Journal of Sedimentary Petrology 59: 361-374.

Milliken, K.L., 2005. Late diagenesis and mass transfer in sandstone-shale sequences. In: Mackenzie, F.T. (Ed.), Treatise on geochemistry 7: Sediments, diagenesis and sedimentary rocks.

Milliken, K.L.2003. Late diagenesis and mass transfer in sandstone—Shale sequences. In Treatise on Geochemistry; Holland, H.D., Turekian, K.K., (Eds.); Elsevier: Amsterdam, The Netherlands, pp. 159-190.

Milliken, K.L.; Ergene, S.M.; Ozkan, A. 2016. Quartz types, authigenic and detrital, in the upper cretaceous eagle ford formation, south Texas, USA. Sediment. Geol., 339: 273-288.

Milliken, K.L., Olson, T. 2017. Silica diagenesis, porosity evolution, and mechanical behavior in siliceous mudstones, Mowry shale (Cretaceous), Rocky Mountains, U.S.A. J. Sediment. Res. 87: 366-387.

Min, H., Zhang, T., Li, Y., Zhao, S., Li, J., Lin, D., Wang, J., 2019. The Albitization of K-Feldspar in Organic- and Silt-Rich Fine-Grained Rocks of the Lower Cambrian Qiongzhusi Formation in the Southwestern Upper Yangtze Region, China, Minerals, 9: 620; doi:10.3390/min9100620.

Morad, S., 1988. Albitized microcline grains of post-depositional and probable detrital origins in Brøtum Formation sandstones (Upper Proterozoic), Sparagmite Region of Southern Norway. Geological Magazine 125: 229-239.

Morad, S., Bergan, M., Knarud, R., Nystuen, J.P., 1990. Albitization of detrital plagioclase in Triassic Reservoir sandstones from the Snorre Field, Norwegian North Sea. Journal of Sedimentary Petrology 60 (3): 411-425.

Morad, S., Ketzer, J.M., De Ros, F., 2000. Spatial and temporal distribution of diagenetic alterations in siliciclastic rocks: implications for mass transfer in sedimentary basins. Sedimentology 47: 95-120.

Neuser, R.D., Bruhn, F., Götze, J., Habermann, D., Richter, D.K., 1995. Kathodolumineszenz:

Methodik und Anwendung. Zentralblatt für Geologie und Paläontologie Teil I 287-306 (H, ½).
Norberg, N., Neusser, G., Wirth, R., Harlov, D., 2011. Microstructural evolution during experimental albitization of k-rich alkali feldspar. Contrib. Mineral. Petrol., 162: 531-546.
Petersson, J., Stephens, M.B., Mattsson, H., Charlotte Möller, C., 2012. Albitization and quartz dissolution in Paleoproterozoic metagranite, central Sweden — Implications for the disposal of spent nuclear fuel in a deep geological repository, Lithos, 148: 10-26.
Pettijohn, F.J., Potter, P.E. Siever, R. 1987. Sand and Sandstone, 2nd ed., New York, Springer-Verlag, 533 pp.
Poursoltani, M.R., Gibling, M.R., 2011. Composition, porosity and reservoir potential of the Middle Jurassic Kashafrud Formation, northeast Iran. Marine and Petroleum Geology 28: 1094-1110.
Poursoltani, M.R., Gibling, M.R., Pe-Piper, G., 2019. Diagenesis, burial history, and hydrocarbon potential of Cambrian sandstone in the northern continental margin of Gondwana: A case study of the Lalun Formation of central Iran. Journal of Asian Earth Sciences 172: 143-169.
Poursoltani, M.R., Pe-Piper, G., 2020. Diagenetic history and provenance of Devonian terrestrial sandstones: Padeha Formation, eastern Alborz, Iran, Chemical Geology, Journal of Asian Earth Sciences, 204: 104576.
Poursoltani, M.R., 2021. Diagenetic history of Cretaceous sandstones of the Neyzar Formation, Kopet-Dagh Basin, NE Iran: a case study of albitization, Arabian Journal of Geosciences, 14: 1164.
Ramseyer, K., Boles, J.R., Lichtner, P.C., 1992. Mechanismof diagenetic albitization. Journal of Sedimentary Petrology 62 (3): 349-356.
Roser, B.P., Korsch, R.J. 1988. Provenance signature of sandstone-mudstone suite determined using discriminant function analysis of major element data. Chem. Geol., 67: 119-139.
Ruban, D.A., Al-Husseini, M.I., Iwasaki, Y., 2007. Review of Middle East Paleozoic plate tectonics, GeoArabia 12(3): 35-56.
Saigal, G.C., Morad, S., Bj rlykke, K., Egeberg, P.K., Aagaard, P., 1988. Diagenetic albitization of detrital K-feldspar in Jurassic, Lower Cretaceous, and Tertiary clastic reservoir rocks from offshore Norway, I. Textures and origin. Journal of Sedimentary Petrology, 58 (6): 3-13.
Stöcklin, J., 1968. Structural history and tectonics of Iran: a review. AAPG Bulletin 52: 1229-1258.
Taylor, T.R., Giles, M.R., Hathon, L.A., Diggs, T.N., Braunsdorf, N.R., Birbiglia, G.V., Kittridge, M.G., Macaulay, C.I., Espejo, I.S., 2010. Sandstone diagenesis and reservoir quality prediction: Models, myths, and reality. AAPG Bull 94: 1093-1132.
Tawfik, H.A., Ghandour, I.M., Maejima1, W., Abdel-Hameed, A.T., 2011. Petrography and Geochemistry of the Lower Paleozoic Araba Formation, Northern Eastern Desert, Egypt: Implications for Provenance, Tectonic Setting and Weathering Signature, Journal of Geosciences, Osaka City University, 54: 1-16.
Turcotte, D.L., Schubert, G. 2002. Geodynamics (2nd ed.). Cambridge, England, UK: Cambridge University Press. 136-7 pp.
Walker, T.R., 1984. Diagenetic albitization of potassium feldspars in arkosic sandstones. J. Sediment. Petrol, 54: 3-16.
Wendt, J., Kaufmann, B., Belka, Z., Farsan, N., Karimu-Bavandpur, A., 2002.Devonian/Lower Carboniferous stratigraphy, facies patterns and paleogeog-raphy of Iran, Part I. Southeastern Iran. Acta Geologica Polonica 52: 129-168.
Wendt, J., Kaufmann, B., Belka, Z., Farsan, N., Karimu-Bavandpur, A., 2005.Devonian/Lower Carboniferous stratigraphy, facies patterns and paleogeog-raphy of Iran Part II. Northern and central Iran. Acta Geologica Polonica 55: 31-97.
Zand-Moghadam, H., Moussavi-Harami, R., Mahboubi, A., 2014. Sequence stratigraphy of the Early-Middle Devonian succession (Padeha Formation) in Tabas Block, East-Central Iran: Implication for mixed tidalflat deposits. Palaeoworld 23: 31-49.